J. Appl. Phys. Supp., **32** [3] 378S–379S (1961).
[5]P. I. Slick, "A Thermogravimetric Study of the Equilibrium Relations between a MnZn-Ferrite and an O_2–N_2 Atmosphere," *Ferrites, Proc. Int. Conf., 1970*, 81–83 (1971).
[6]J. M. Brownlow, "Preferential Volatilization of Cations from Ferrites During Sintering," *J. Appl. Phys.*, **29** [29] 373 (1958).
[7]A. Beer and J. Schwarz, "New Results on the Influence of Sintering Conditions on the Properties of MnZn-Ferrites," *IEEE Trans. Magn.*, **2** [3] 470–72 (1966).
[8]N. J. Hellicar and A. Sicignano, "Dynamic Role of Zinc Oxide in the Sintering of Manganese Zinc Ferrites," *Am. Ceram. Soc. Bull.*, **61** [4] 502–505 (1982).
[9]D. Condurache, C. Pasnicu, and E. Luca, "On the Kinetics of the Vaporization of Zn Ions in the Sintering Process of Ferrites"; pp. 157–61 in Advances in Ceramics, Vol. 15. Edited by F. Y. Wang. American Ceramic Society, Columbus, OH, 1985.
[10]P. Sainamthip and V. R. W. Amarakoon, "Preparation of Manganese Zinc Ferrite Powders by Alcoholic Dehydration of Citrate/Formate Solution," *J. Am. Ceram. Soc.*, **71** [2] C-92–C-95 (1988).
[11]P. Reijnen, "Phase Equilibria in the System MgO–FeO–Fe_2O_3," *Philips Res. Rep.*, **23**, 151–88 (1968).
[12]A. L. Stuijts, "Control of Microstructures in Ferrites," *Ferrites, Proc. Int. Conf., 1970*, 108–13 (1971).
[13]B. K. Das, "Developments in Preparation of Soft Ferrites"; p. 96 in Preparation and Characterization of Materials. Edited by J. M. Honig and C. N. R. Rao. Academic Press, New York, 1981.
[14]P. I. Slick and H. Basseches, "Thermogravimetric Study of the Solid–Gas Interaction of a MnZn-Ferrite and the Effect on Its Magnetic Properties," *IEEE Trans. Magn.*, **2** [3] 603–607 (1966).
[15]G. Schnitt and P. Kleinert, "Studies on Material Transport during the Formation of Zinc and Nickel Ferrite from the Oxides. II. On the Role of the Gas Phase for the Material Transport during the Ferrite Formation," *Z. Anorg. Allg. Chem.*, **398**, 41–53 (1973).
[16]E. Roess, "Magnetic Properties and Microstructure of High-Permeability MnZn-ferrites," *Ferrites, Proc. Int. Conf., 1970*, 203–209 (1971).
[17]R. C. Sundahl, Jr., B. B. Ghate, R. J. Holmes, and C. E. Pass, "The Grain Boundary Chemistry and Magnetic Properties of $Mn_{0.5}Zn_{0.42}Fe_{2.08}O_4$"; pp. 502–11 in Advances in Ceramics, Vol. 1. Edited by L. M. Levinson. American Ceramic Society, Columbus, OH, 1981.
[18]M. Drofenik, S. Besenič ar, M. Limpel, and V. Gardaševič, "Influence of the Dimensions of MnZn-Ferrite Samples on Their Microstructural and Magnetic Properties"; pp. 229–36 in Advances in Ceramics, Vol. 15. Edited by F. Y. Wang. American Ceramic Society, Columbus, OH, 1985. □

J. Am. Ceram. Soc., 71 [8] 648–57 (1988)

Transformation Plasticity of CeO_2-Stabilized Tetragonal Zirconia Polycrystals: II, Pseudoelasticity and Shape Memory Effect

PATRICIO E. REYES-MOREL,*,† JYH-SHIARN CHERNG,* and I-WEI CHEN*

Department of Materials Science and Engineering, University of Michigan, Ann Arbor, Michigan 48109–2136

A macroscopic shape memory effect is demonstrated by first deforming a CeO_2-stabilized tetragonal zirconia polycrystal (Ce-TZP) between the M_b and A_s temperatures and then recovering the shape change by heating above A_b. Shape changes effected above A_b are immediately recoverable during unloading, giving rise to a pseudoelastic behavior. Deformation texture is reversible when the shape strain recovers. Both M_b and A_b, along with the associated temperature range for these effects, are depressed to lower temperatures by grain refinement. Prior deformation widens the gap between the transformation temperatures. These observations demonstrate that the shape accommodation in Ce-TZP arises from twinning and elastic distortions. The operation of pseudoelasticity and shape memory effect is rationalized in terms of martensitic nucleation statistics, the stability of thermoelastic martensite, and internal stresses at the martensitic interface. The implications on transformation plasticity and transformation toughening are explored.

I. Introduction

In the previous paper,[1] we have demonstrated that transformation plasticity in Ce-TZP is related to a stress-assisted tetragonal-to-monoclinic (*t*-to-*m*) transformation and that its yield stress has a positive pressure and temperature sensitivity. Other aspects of the constitutive relation and the associated experimental observation have been detailed in terms of statistics of single-site and multiple-site nucleation. Yet, how the large shape distortion of the transformation is accommodated inside the ceramic is not evident from these considerations. The latter issue is an important one for understanding transformation plasticity and is the subject of the present paper.

In principle, the shear and dilatation caused by the *t*-to-*m* transformation can be either elastically or plastically accommodated by dislocation motion, twinning, and microcracking. Although evidence for operation of the above exists for transformation-toughened zirconia ceramics, the relative importance of the respective mode of accommodation remains to be quantified. A direct way to probe the nature of shape accommodation in transformation plasticity is by studying the reverse *m*-to-*t* transformation. In particular, if the reverse *m*-to-*t* transformation also causes a reversal of the macroscopic shape strains, one may logically conclude that the primary modes of strain accommodation are themselves microscopically reversible. Of the plastic processes mentioned above, only twinning is reversible. Elastic distortions, of course, are always reversible and, indeed, may direct the reverse motion of twin interfaces.

This paper documents our observations of the shape reversals during reverse transformations in deformed Ce-TZP. For reference, a temperature–transformation curve of Ce-TZP reported in the earlier paper is reproduced schematically in Fig. 1.[1] The *t*-to-*m* transformation is initiated by a large burst, at the M_b temperature, followed by further transformation as the temperature is reduced. During heating, the reverse transformation starts at A_s, but a nearly complete *m*-to-*t* reversion burst usually occurs at a higher temperature A_b. Referring to this plot, two types of shape reversal effects were envisioned and sought in the present study. First, when initially deformed between M_b and A_s, a test piece may retain its macroscopic shape strain during unloading but later reverse it upon subsequent heating above A_b. This is termed the shape memory effect.[2] Second, when initially deformed above A_b, a test piece may reverse its macroscopic shape strain during unloading. This is termed pseudoelasticity.[2] Introductory explanations of these effects in metallic alloys can be found elsewhere.[2,3]

Several reports in the recent literature are indicative of the shape memory effects in zirconia ceramics. Coyle[4] suspected that the high toughness of Ce-TZP (15 to 18 mol% CeO_2) was due to a stress-driven transformation occurring near the crack tip which

Manuscript No. 199775. Received August 27, 1987; approved February 15, 1988.
Presented at the 89th Annual Meeting of the American Ceramic Society, Pittsburgh, PA, April 28, 1987 (Basic Science Division, Paper No. 115-B-87).
Supported by the National Science Foundation under Grant No. 8407868/8609146; support for P. E. Reyes-Morel provided in part by the Chilean government.
*Member, the American Ceramic Society.
†Also in the Department of Nuclear Engineering.

reversed after the crack passed by. He could offer no definitive evidence, however, because no trace of monoclinic phase was detected anywhere in his material except around hardness indents. This observation was discussed extensively in the review of Evans and Cannon, and a dilatational toughening prediction in the presence of a reversible transformation was presented.[5] Marshall and James reported a reversible stress-induced transformation in magnesia-partially-stabilized zirconia (Mg-PSZ) based on optical observations and X-ray measurements on a stressed surface.[6] Marshall found,[7] however, that the unloading stress–strain curve recorded by strain gauges was entirely linear; thus the reversible transformation on the free surface had only a negligible effect on macroscopic deformation. Indeed, the surface X-ray measurements of Marshall and James[6] revealed a mere 1% to 4% monoclinic content variation during load cycling, while the background monoclinic content on the specimen surface was already 14% before loading. Strictly speaking, the above two reports[4,6] were at most indicative of a reversible transformation upon unloading, but offered no evidence for shape recovery which requires a recovery of deviatoric (shear) strain. A first claim of a shape memory effect in zirconia ceramics was made by Swain,[8] who observed the shape recovery of a bent Mg-PSZ bar upon heating above a certain temperature. His claim is not justifiable, however, since even a reverse dilatational transformation upon heating above A_b can cause reverse bending, due to the fact that a bent zirconia bar yields by transformation on the tensile side only,[1,7,9] leaving an asymmetric residual stress.[7] Thus the observed shape recovery was fortuitous and could not be regarded as a manifestation of a shape memory effect itself. Lastly, attempts to provide evidence for shape memory effects using in situ TEM have not been entirely successful either. In the study of Mg-PSZ by Hannink, Porter, and Marshall, it was specifically reported that precipitates transforming back and forth between the monoclinic and tetragonal structures had no memory of their prior twin configurations,[10] presumably because of the complicated thin foil stresses which were difficult to control in this type of beam-heating, beam-stressing experiment. After extended beam heating of an initially cubic region, though, they observed the cubic region turned into a tetragonal one in which several laths retracted and regrew following the same path. The latter experiment, however, entailed a significant redistribution of solutes in the beam-heated region, evidenced by the conversion of the cubic phase into the tetragonal phase and even MgO forming on surrounding regions of the foil. Hence the memory of the lath growth could be attributed to a spatial gradient of the solute concentration which biased the chemical stability of zirconia phases. Taken in toto, we do not believe that the above results and discussions[4,6,8,10] in the literature have constituted convincing evidence for a macroscopic shape memory and pseudoelasticity effect in zirconia ceramics. In the present study we hope to fully demonstrate these features.

Until now, the stability of t and m phases has been definitively assessed only through the t-to-m transformation, drawing on the concept of heterogeneous nucleation and nucleation statistics.[11–15] The stability of the monoclinic phase in the m-to-t transformation is thought to be more complicated and has received little consideration. The discovery of shape memory effects allows us to treat the latter problem more rigorously, based on the notion of thermoelastic equilibrium of the monoclinic plate.[16,17] This aspect of the phase stability, and the related issues in transformation, transformation plasticity, and transformation toughening, will be explored accordingly.

II. Experimental Procedure

The materials studied here are several Ce-TZPs containing 12 mol% CeO_2. One batch with a grain size varying from 0.96 to 2.8 μm was sintered between 1400° and 1600°C using a commercial powder; the other batch with a grain size of 1.2 μm was received in the as-sintered form from a different source. At these grain sizes, Ce-TZPs were entirely made of transformable tetragonal phase in the as-sintered condition. The thermomechanical properties of the above materials have been fully characterized in our laboratory and reported in previous studies.[1,18]

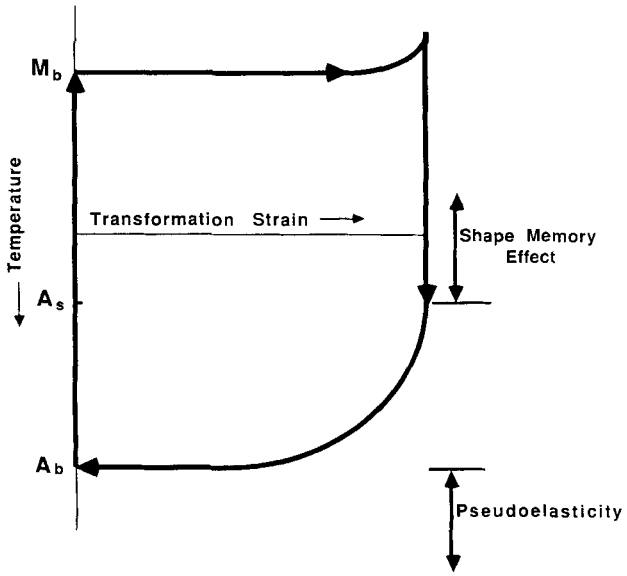

Fig. 1. Schematic transformation curve for Ce-TZP, with the temperature regimes for the two types of shape memory effects indicated on the right.

Relatively large strains are generally desired to demonstrate the shape memory effects. Hence, the shape deformation in this study was primarily effected by uniaxial compression and, in a few cases, by hydraulic compression.[1,18] In the latter experiment, a hydrostatic pressure was superimposed onto the uniaxial compression, to suppress fracture in order to achieve larger strains. Axial and radial strain gauges were used to record volumetric and shape strain evolution during loading, unloading, and subsequent heating. All the stress–strain curves reported in this paper were recorded using a servo-controlled machine. Details of the above experimental procedures have been given elsewhere.[1,18] Standard X-ray diffractometry using Cu$K\alpha$ radiation and dilatometry were also employed to evaluate t-to-m transformation.

III. Results

(1) Shape Memory Effect

A typical shape memory effect is illustrated in Fig. 2. This material is a Ce-TZP of a relatively large grain size (2.8 μm). Under uniaxial compression at room temperature, it deformed plastically owing to the t-to-m transformation. Stable deformation was interrupted by repeated load drops, at a nearly constant upper yield stress. After complete unloading, only a small reverse plastic flow of the axial strain was evident. Subsequent heating produced a gradual recovery of the axial strain due to the m-to-t reversion starting at 60°C, and a burst of strain recovery at 186°C. The burst was sharp, thus permitting the designation of A_b, above which approximately 95% of the prior axial strain had been recovered. A similar recovery of the radial strain, from an expansion in compression to a contraction in heating, was also observed. Taking the axial and radial strains together, which are of the opposite sense to each other in compression tests, we verified that the volume increased during deformation but decreased during heating, as expected for forward and reverse t-to-m transformations.

The shape memory effect was found in Ce-TZP of finer grain sizes as well. As shown in Fig. 3, in similar experiments of various prior axial strains up to 1%, heating to A_b produced a 90% shape recovery for grain sizes ranging from 1.0 to 2.8 μm. It should be noted that the yield stress and A_b depend sensitively on the grain size, as will be shown later in this section. Thus, the shape memory effect apparently exists in Ce-TZPs of different microstructures (i.e., grain size d), of different strengths, and at different chemical

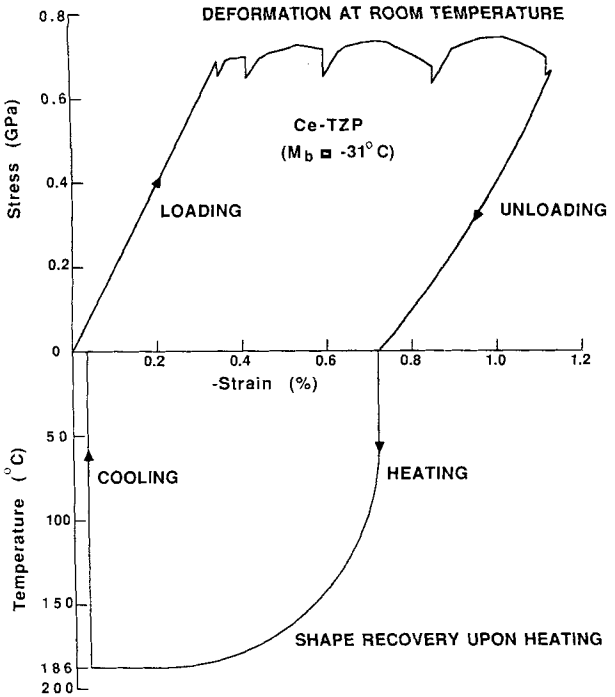

Fig. 2. Axial stress–strain curve for Ce-TZP (M_b = −31°C) under uniaxial compression at room temperature, together with temperature–strain curve showing strain recovery on heating.

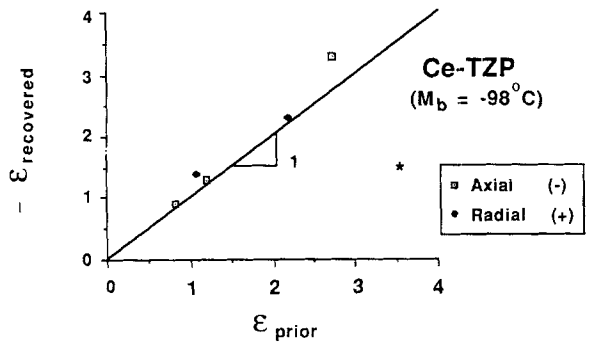

Fig. 4. Recovered strain versus prior deformation showing nearly 100% recovery in both axial and radial directions. The radial strain marked ★ did not fully recover because of the presence of axial cracks.

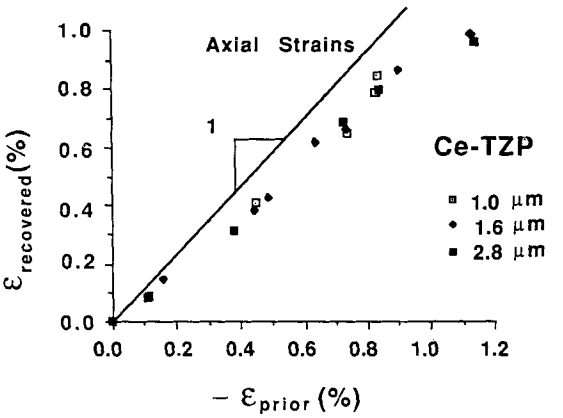

Fig. 3. Recovered strain versus prior deformation showing nearly 90% shape memory. Only axial strains are plotted.

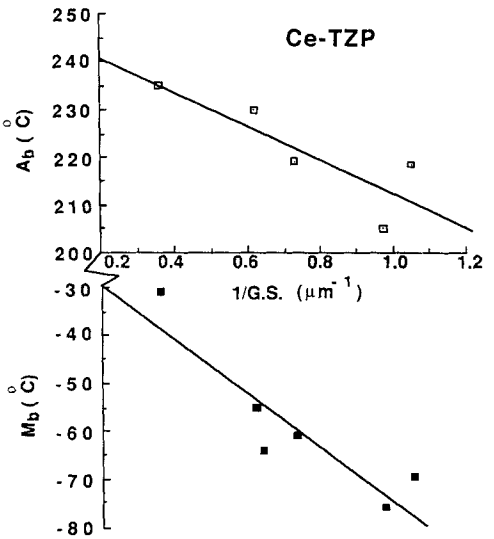

Fig. 5. Grain-size dependence of A_b and M_b of Ce-TZP.

driving forces g_{ch}—the latter three are of course interrelated.

At room temperature, uniaxial compression beyond 1% strain tends to generate excessive microcracks, thus resulting in irreversible damage, premature fracture, and degradation of shape memory. To overcome such problems, several samples deformed in hydraulic compression were also examined. In hydraulic compression, microcracking is substantially stabilized to delay failure.[18,19] Thus, axial compressive plastic strains up to 4.5% could be obtained. The results from these more heavily deformed samples are shown in Fig. 4. Except for the radial strain of one specimen which reached a large initial deformation strain, a nearly 100% shape recovery at A_b was verified in all other cases. (The unrecovered radial strain in the exception can be attributed to microcracking which aligns along the axial direction.) Note that the recorded volumetric dilatation at the axial strain of 2.74% was 4.36%, indicating that the majority of the tetragonal volume had already transformed. The flow stress in the latter case was much higher, and the deformation was well into the final strain hardening regime described in the previous paper.[1] Thus, the shape memory effect apparently persists in all stages of transformation plasticity in Ce-TZP.

(2) Grain Size and Strain Dependence

Shape memory effects were found in Ce-TZP of different grain sizes, and the extent of strain recovery was independent of the grain size. Transformation temperatures, however, are sensitive to microstructure. Specifically, we found that both M_b and A_b were depressed by grain refinement, as shown in Fig. 5. Since M_b is lowered by grain refinement, it should be expected that the yield stress will increase as described in the previous paper.[1] This is illustrated in Fig. 6, which reconfirms the operation of stress-assisted transformation. Therefore, grain refinement has the dual effect of elevating the stress regime but lowering the temperature regime over which the shape memory effects operate.

A related aspect concerning strain dependence of the transformation temperatures was investigated. As reported in the previous paper,[1] M_b is not dependent on prior strain if the deformation is in stage I, but a prior strain beyond stage I will supress burstlike transformations in subsequent cooling.[1] These results were rationalized in terms of the nucleation statistics of autocatalysis in the previous paper. The A_b dependence on prior deformation is reported here. In slightly deformed samples, the first burst of *m*-to-*t* transformation always occurred at a lower temperature than the normal A_b measured in an undeformed sample previously cooled below M_b. However, this lower burst temperature rapidly increased with

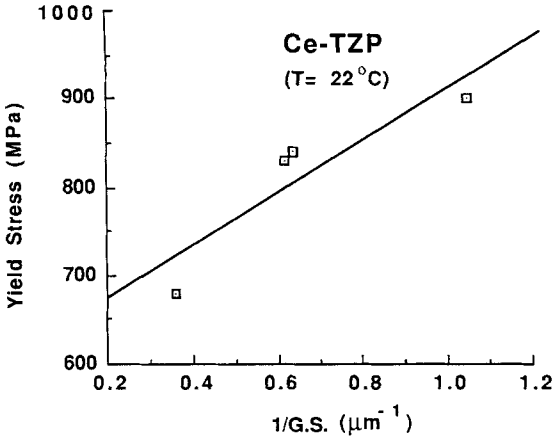

Fig. 6. Grain-size dependence of compressive yield stress of Ce-TZP.

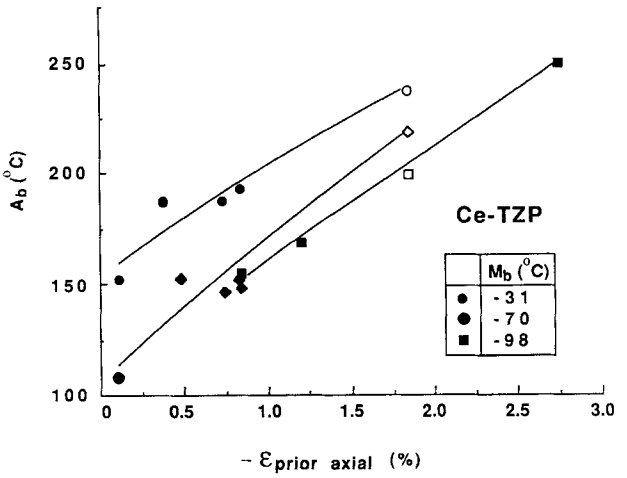

Fig. 7. A_b temperature versus the amount of prior deformation for samples with different M_b. Open symbols represent A_b of samples previously transformed at M_b.

the prior deformation. This trend is shown in Fig. 7 for three materials, including data for one material which was hydraulically compressed to much larger strains. The normal A_b temperatures of the three materials, measured by going through the cooling cycle below M_b before heating, are shown in Fig. 7 as open symbols. The latter data would be consistent with the data of predeformed specimens, if a prior strain around 1.7% could be assigned to them. Note that transformation at M_b alone involves a volumetric expansion around 3.3%, corresponding to a 66% *t*-to-*m* conversion. From deformation studies described in Fig. 8 of the previous paper,[1] we estimate that, to generate a comparable *t*-to-*m* conversion and volumetric expansion, an equivalent uniaxial strain around 1.5% would be required, as indeed suggested by Fig. 7. Thus, a thermally cycled sample first transforming at M_b rather resembles a substantially deformed material.

(3) Phase Identification and Textures

Previous studies in our laboratory have definitively identified the transformation plasticity in zirconia ceramics with the *t*-to-*m* transformation. A texture of both phases was reported and attributed to the stress bias in the stress-assisted transformation.[1,20,21] This connection dictates that the shape memory effects due to stress-assisted transformation must be accompanied by a texture memory governing orientations of microscopic phase variants.

Initially, at an instrument resolution of 5%, no detectable monoclinic phase and no texture of the tetragonal phase were found in the undeformed samples. In the deformed state, the monoclinic phase was identified. This is documented in Fig. 8 for the amount of surface monoclinic content estimated from standard X-ray diffractometry using peak height ratios of {111} reflections. Despite some scattering, the amount of monoclinic content as bounded by the two lines in Fig. 8 increases with deformation strain. A texture was also found in the deformed state, as can be seen from Fig. 9, which plots the diffracted intensities of {113}, {220}, {200}, and {111} reflections of the axial and radial cross sections in the deformed and the recovered states. The textures of both *t* and *m* phases in this case were distinct and typical of a deformed TZP or PSZ. Later, after heating above A_b, the *m* phase disappeared as did the texture of the *t* phase, as clearly shown in Fig. 9. These results confirmed that the shape memory was accompanied by a texture memory in the present material.

(4) Pseudoelasticity

When uniaxial compression is conducted above A_b, plastic strain recovers during unloading. This is demonstrated in Fig. 10 from an experiment performed at 210°C for both the axial and radial strains. Several features of pseudoelasticity are notable in Fig. 10. First, unlike transformation plasticity at room temperature, no load drop or flat, plastic regime was observed. Instead, a stable regime of gradual strain hardening was found. The volume of the specimen

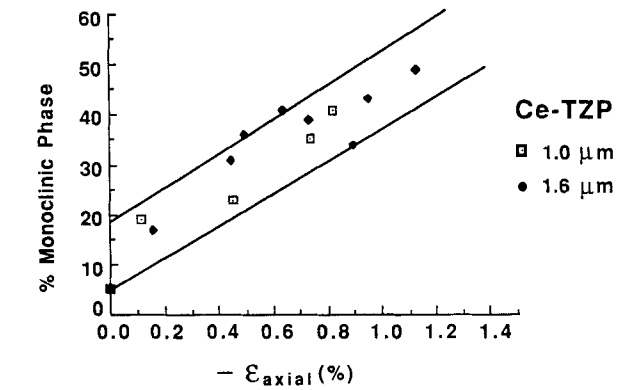

Fig. 8. Amount of surface monoclinic phase estimated from XRD as a function of axial strain.

increased during this stage. Second, even after stress reversal, forward plastic deformation proceeded for a while, albeit at decreasing stresses, as shown by the post-peak-stress portions of the stress–strain curves. This feature is consistent with our other observations, e.g., stress relaxation,[1,18] strain rate sensitivity,[1] and creep,[22] which are indicative of the presence of long-range internal stresses and a requirement for thermal activation in transformation plasticity.[18] The volume of the specimen continued to increase during this stage. Third, following the initial forward strain during unloading, the reversal of strains at some point has an unloading tangent modulus approaching the elastic constants. The volume of the specimen began to decrease during this stage, by virtue of elastic contraction. Fourth, below a certain stress, unloading was increasingly dominated by the reversal of the plastic strains. The volume of the specimen decreased rapidly during this stage. Finally, the last portion of the pseudoelastic loop is again elastic, with the expected elastic constants and elastic contraction. At this point, the shape recovery for the radial plastic strain was 98%. The slightly lower recovery of the axial plastic strain was due to the irreversible closure of sintering pores, which were susceptible to axial collapse in compression.

We also investigated the effect of cycling on the pseudoelastic effect at 210°C. As shown in Fig. 11, prior pseudoelastic deformation caused a lowering of the initial yield stress and a narrowing of the hysteresis loop. Such effects were most prominent in the first few cycles and seemed to saturate afterward. A small amount of unrecovered strain remained after each cycle, causing strain accu-

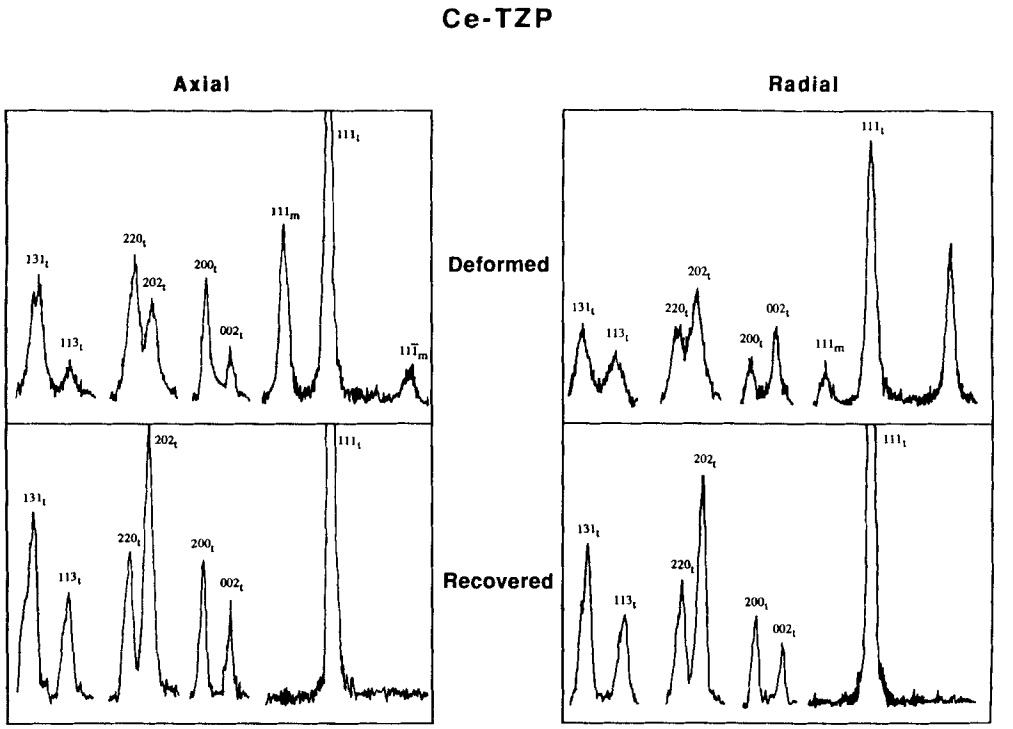

Fig. 9. Textures of monoclinic and tetragonal phases in the deformed and recovered states.

mulation. Although permanent plastic strain accumulates slowly, ~0.1% per cycle at the amplitude shown in Fig. 11, microcracking does occur in pseudoelasticity just as in transformation plasticity at lower temperatures.[1,18] Typically, after five or six cycles at the present amplitude, the specimen failed.

The effect of temperature on the yield stress in transformation plasticity has been documented previously.[1] At lower temperatures near M_b, a steep positive temperature dependence was observed, as can be rationalized by a stress-assisted transformation.[1] This positive temperature dependence continues to be observed in the regime of pseudoelasticity, as the data in Fig. 12 indicate. Thus the onset of yield in pseudoelasticity is also stress-assisted. Indeed, the very occurrence of transformation above A_b under stress is a manifestation of stress-assisted transformation. The effect of temperature and cycling on pseudoelasticity is shown in Fig. 13, with successive stress–strain curves of a specimen loaded at progressively lower temperatures. The temperature dependence of the yield stress is evident from these plots. Below 140°C, pseudoelasticity was not observed. Note that the amount of postpeak forward deformation also decreased with lower temperatures, and a more extended elastic unloading preceded the reverse plastic deformation. However, even at room temperature or slightly below, some reversed plastic flow was recorded.

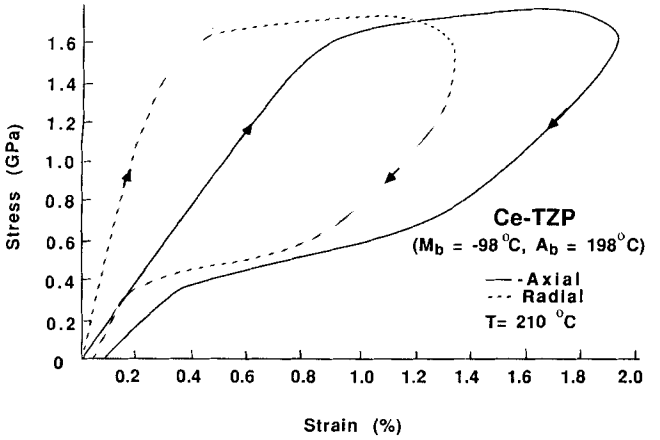

Fig. 10. Stress–strain curves for Ce-TZP under uniaxial compression at 210°C showing pseudoelasticity. $\dot{\varepsilon} = 3 \times 10^{-5}\ s^{-1}$.

IV. Thermoelastic Martensitic Transformation

Our observations of the shape memory effects in Ce-TZP can be understood in terms of the classical theory of martensitic nucleation and growth. To set the stage of discussions, we first outline

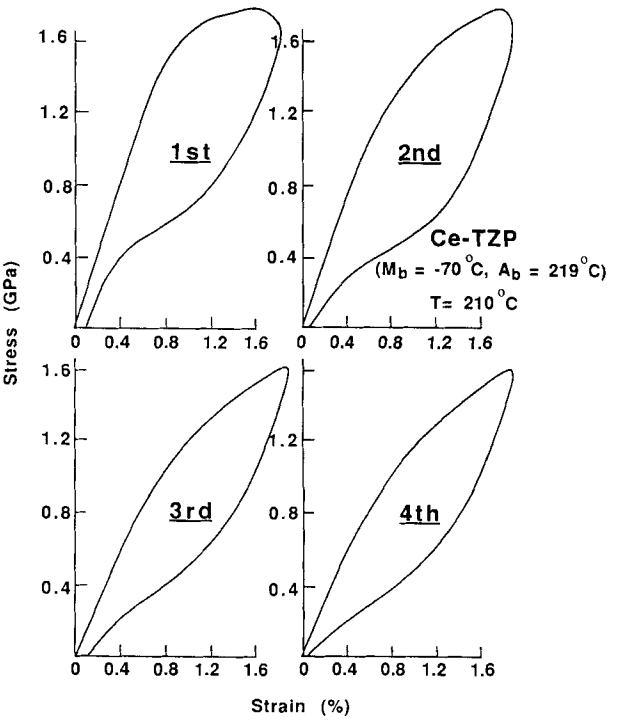

Fig. 11. Axial stress–strain curves for Ce-TZP showing pseudoelasticity at 210°C for different cycles. $\dot{\varepsilon} = 3 \times 10^{-4}\ s^{-1}$, G.S. = 0.95 μm.

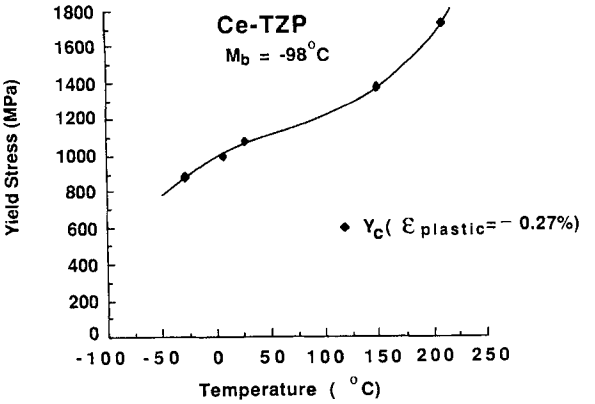

Fig. 12. Positive temperature dependence of yield stress for Ce-TZP.

the basic elements of this theory, which has been previously applied by Chen, Chiao, and Reyes-Morel to zirconia transformations.[1,11–15,18] For simplicity, in the following treatment, only stress-free transformation will be considered. Its extension to stress-assisted transformation is straightforward given the formulation developed in the previous paper equating stress assistance to a part of the driving force.[1]

As shown by Chen and Chiao,[12,14] the free energy ΔG of a monoclinic plate in a tetragonal matrix can be represented by

$$\Delta G = (4\pi/3)r^2t(g_{ch} + g_{str} + Kt/r) + 2\pi r^2\gamma \quad (1)$$

Here, we have assumed a nucleus in the form of an oblate spheroid lying perpendicular to the **x** axis, with a radius r and a semithickness t, such that the simple shear direction is along the **z** axis. In this form, g_{ch} is the chemical driving force for the phase change, Kt/r is the shape-dependent strain energy of a plate lying perpendicular to **x**, g_{str} is the excess strain energy from the distortion of the **y**–**z** plane, and γ is the coherent interfacial energy of the m/t interface. Expressions of g_{str} and K are listed in the Appendix, following the standard solution given by Christian.[23]

As shown several times in the literature,[24,25] the three-dimensional plot of the free energy of the plate versus its size parameters has a nucleation barrier around the origin, with a saddle point located at

$$r^* = 4\gamma K/(g_{ch} + g_{str})^2 \quad (2a)$$

$$t^* = -2\gamma/(g_{ch} + g_{str}) \quad (2b)$$

The nucleation barrier, $\Delta G^*(c^*, r^*)$, is

$$\Delta G^* = 32\pi\gamma^3K^2/3(g_{ch} + g_{str})^4 \quad (3)$$

The saddle point corresponds to the configuration of the critical nucleus in homogeneous nucleation. It also corresponds to the smallest monoclinic plate which is thermoelastically stable against the m-to-t reversion. Using appropriate lattice parameters and thermodynamic properties for zirconia, the predictions of the above considerations for the stability of a monoclinic plate are illustrated for pure zirconia in Fig. 14, taken from Chen and Chiao.[12] Two salient features are revealed: (a) an existing monoclinic plate of a larger radius, e.g., 0.3 μm, is thermoelastically stable up to a rather high temperature, e.g., 1000 K; and (b) without a preexisting nucleus, the homogeneous nucleation of a monoclinic plate will face an insurmountable barrier. We shall assume that the depicted behavior in the figure is at least qualitatively representative of Ce-TZP. To utilize these plots for the present application, we simply need to shift the temperature scale downward so that the equilibrium temperature T_0 coincides with that of the 12 mol% CeO_2–ZrO_2.[26]

As shown by Chen and Chiao, heterogeneous nucleation is required in all cases known to effect the t-to-m transformation.[11–15] The probability of heterogeneous nucleation, which requires the

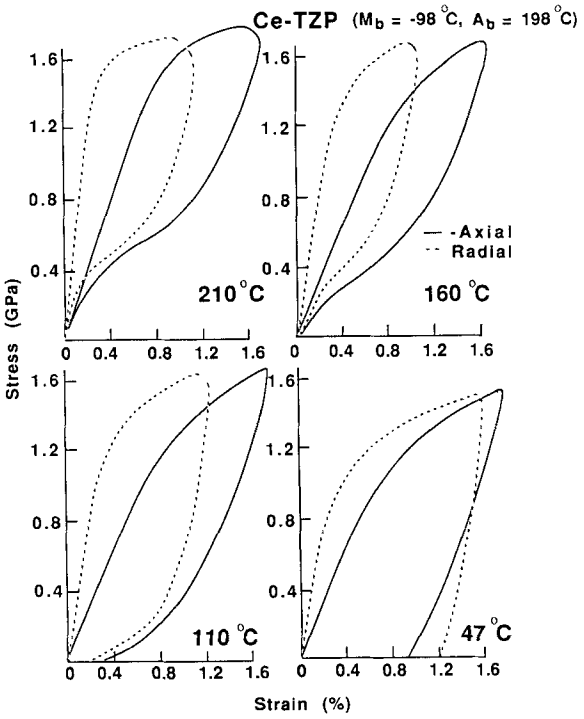

Fig. 13. Stress–strain curves for Ce-TZP showing pseudoelasticity at higher temperatures. $\dot{\varepsilon} = 3 \times 10^{-4}\ s^{-1}$.

presence of a nucleation site, depends on the particle size and the driving force. From a data analysis of martensitic nucleation, they found the probability of the t-to-m transformation to be well represented by the following form:[15]

$$F = 1 - \exp(-Cd^2) \quad (4)$$

where d is the particle size and C is a parameter which increases quadratically with the driving force. Equation (4) predicts that the probability of nucleation in a single particle increases with particle size and decreases with temperature, which can be rationalized in

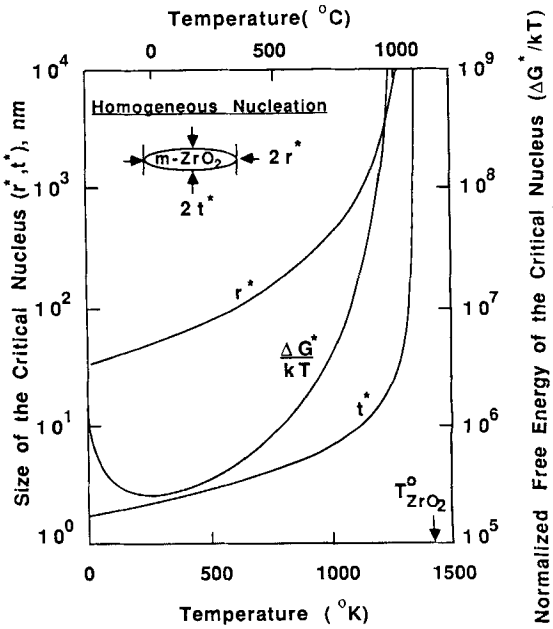

Fig. 14. Free energy, radius, and thickness of a monoclinic critical nucleus in tetragonal ZrO_2.

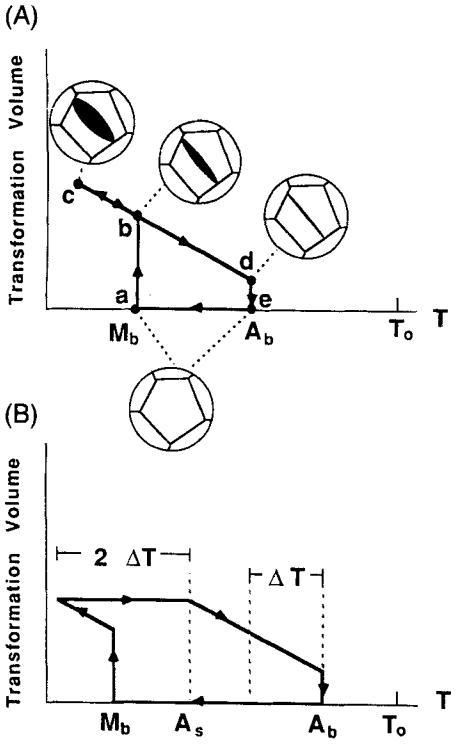

Fig. 15. Predicted transformation curves (*A*) without and (*B*) with friction. Insets in (*A*) illustrate a matrix grain with a transforming variant at various stages. Effect of friction is schematically shown by a temperature increment ΔT.

terms of the probability of finding a potent heterogeneous nucleating defect in a finite space.[15]

The above formulation was originally developed for martensitic nucleation in a single particle, in which the concept of thermoelastic equilibrium is appropriate at the size scale of a critical nucleus and the statistical consideration is straightforward for a highly undercooled isolated particle. However, if elastic accommodation continues to dominate at a larger size scale than the critical nucleus, the concept of thermoelastic equilibrium can be applied to later stages of transformation as well. For polycrystals, we will also (a) assume that only plates of self-similar geometry form in all the grains and (b) include the effects of autocatalysis by considering statistics of multiple-site nucleation.[1] With the above considerations, we proceed to interpret features of the transformation curve, e.g., Fig. 1.

First, treating each grain as an individual particle following the statistics of Eq. (4), we find the probability of multiple-site nucleation proportional to F^n, where n, larger than unity, is determined by the number of participating grains in a critical nucleation event.[1] To attain autocatalysis, a critical probability sharply dependent on the grain size and undercooling is thus expected. We suggest that this nucleation condition determines M_b and its grain size dependence shown in Fig. 5. Once nucleated, the monoclinic plate has a large excess *radial and through-thickness* driving force, which should allow it to rapidly expand into the metastable tetragonal matrix. Subsequently, its radial growth is first impeded by grain boundaries when $r = d/2$, but the thickness growth continues until $\partial \Delta G/\partial t = 0$ at this radius, reaching an equilibrium thickness given by[16]

$$t = -d(g_{ch} + g_{str})/2K \tag{5}$$

Further cooling below M_b may result in additional growth by thickening of the existing plates according to Eq. (5). We suggest that this growth condition determines the postautocatalysis transformation curve below M_b. (Although cooling below M_b may also stimulate nucleation from less favorable sites in other grains and/or in between monoclinic plates, autocatalysis is now severely limited because the retained tetragonal domains are already finely partitioned and isolated by the monoclinic plates formed at M_b, as we discussed in the previous paper.)[1] Upon heating, the reverse m-to-t transformation begins by thickness contraction in order to satisfy Eq. (5). This contraction continues steadily until the plate reaches the critical, saddle-point configuration. For $r^* = d/2$, the saddle point is reached when the driving force reduces to

$$g_{ch} + g_{str} = -(8\gamma K/d)^{1/2} \tag{6}$$

At this point, the monoclinic plate is unstable against the m-to-t reversion. Thus, it shrinks away rapidly. We suggest that this stability condition determines A_b and its grain size dependence shown in Fig. 5. The above sequence of events is best illustrated by an ideal transformation curve shown in Fig. 15(*A*). In this figure, the first appearance of the monoclinic phase at M_b and the spontaneous growth under the excessive radial and through-thickness driving force thereupon, delineated as a–b, is determined by the site statistics of nucleation. The stability regime of the monoclinic phase, delineated as c–d, is governed by the thermoelastic equilibrium condition at a fixed plate radius according to Eq. (5). The final disappearance of this phase at A_b, delineated as d–e, is determined by the other thermoelastic equilibrium condition at the saddle point, Eq. (6). The concept of Fig. 15(*A*) was first introduced by Olson and Cohen based on a similar reasoning for a single plate nucleus.[16,17]

It is implicit in the above discussion that the m/t interface is completely glissile,[16,17] capable of adjusting its position freely to respond to the driving force. In reality, interface motion is likely to encounter friction, which must be overcome with a finite driving force. (Further discussions of the origins of interface frictions will be given in Section V(1).) In the forward transformation, an additional undercooling is needed to push the m/t interface into the metastable tetragonal matrix. Thus, M_b is depressed further. Friction also impedes the reverse transformation, such that plate thinning does not take place immediately upon heating, but is delayed until A_s when the requisite driving force is available to overcome the interface friction in the reverse motion. Likewise, A_b is elevated. The modified transformation curves to include frictional resistance were also constructed by Olson and Cohen and replotted here as Fig. 15(*B*).[16,17] For polycrystals, further refinement of these constructions is necessary to account for multiple nucleation and growth. While the details depend on the specific case considered, qualitatively, they tend to smooth out the transformation curve overall.

The above considerations, along with the concept of stress-assisted transformation, allow us to make the following predictions concerning martensitic transformation and transformation plasticity in a thermoelastic material. First, both M_b and A_b should decrease with decreasing grain size. Physically, the depression of M_b reflects the need for a larger driving force to compensate for the less favorable nucleation statistics in smaller particles, according to Eq. (4), while the depression of A_b reflects the lower thermoelastic stability of smaller plates which have a larger proportion of interfacial energy, according to Eq. (6). Second, the yield stress at a given temperature should increase with decreasing grain size, and, for stress-driven transformation above A_b, the removal of the external stress should destabilize the monoclinic plate resulting in an m-to-t reversion. Third, prior deformation should not depress M_b but should elevate A_b. Physically, M_b is constant because the statistics of multiple-site nucleation has a very sharp temperature dependence,[1] while A_b is elevated because frictions arise from prior deformation via the residual long-range internal stresses. (The latter point will be discussed in the next section.) Fourth, if only elastic accommodation and twinning are involved in the above processes, then the shape strains and the variant crystallographic orientations should both be reversible, manifesting a perfect shape and texture memory. This would be expected, despite a modest friction, for glissile m/m and m/t interfaces whose reverse motions under favorable driving forces are necessarily directed by elastic distortions inherited from the forward transformation shape strains.

The above predictions are all in qualitative agreement with the experimental observations in Ce-TZP. Thus a reasonably comprehensive picture for transformation, transformation plasticity, shape memory, and pseudoelasticity in Ce-TZP seems to be at hand. Some rudimentary estimations can also be made from the data of A_b to test the internal consistency of the above picture. The extrapolated A_b at zero prior deformation in Fig. 7 will be taken as the temperature at which a monoclinic plate of the respective radius, $r^* = d/2$, becomes thermodynamically unstable. Friction at such small strain is likely to be smaller. From Fig. 14, we can estimate that at $d = 2r^* = 1$ μm, it is approximately 330°C below T_0. For $d = 1$ μm, $A_b = 90$°C at zero prior strain; hence a lower bound estimate of T_0 is 420°C. From the extrapolated t/m phase boundaries on the phase diagram of CeO_2 and ZrO_2, we estimate a T_0 for 12 mol% CeO_2 around 500°C,[26] which is 80°C higher than our lower bound estimate. We also found from Fig. 7 that friction increases with strain and may shift the A_b by another 80°C. Lastly, the temperature difference between A_b and M_b is 280°C, which is more than twice the friction level. As apparent from Fig. 15(*B*), $(A_b - M_b)/2$ places an upper bound on the friction.

V. Discussion

(1) Interface Motion

An essential aspect of martensitic transformation relevant to the present study of transformation plasticity is the nature of interface motion, and its relation to elastic and plastic accommodation. The in situ TEM study of Chiao and Chen on the martensitic interface between monoclinic and orthorhombic phases revealed that the interface is coherent, composed of regularly spaced ledges with a step height of one lattice plane spacing, and that a strain field is associated with each such step.[14,27] The interface migrates steadily, at a constant driving force, by a coordinated glide motion of ledges. This process is responsible for martensitic growth, or shrinkage, at all stages. Note that the ledges, which are associated with a strain field, are themselves interface dislocations. Therefore, they may interact with a stress field, and their glide, say via double-kink formation, may require a sufficient stress bias or a thermal activation. In this sense, an interface friction during motion can be envisioned. Like dislocations, there will be both an athermal and a thermal component of interface friction, and the likely sources of these components can be identified following the standard analysis of dislocation motions.[28] First, the direct observation of interface motion at a constant subsonic velocity at a finite driving force provided direct evidence of a thermal component of interface friction.[14,27] The reported activation volume in transformation plasticity, deduced from stress relaxation and strain rate sensitivity experiments,[1,18] is about 10 times the unit-cell volume, which suggests a double-kink mechanism for the thermal component of interface friction.[28] On the other hand, the athermal component of interface friction arises from a long-range internal stress field which interacts with interface dislocations.[28] Since the latter component dictates the increase of A_b, which in turn increases with prior deformation and prior transformation, it is plausible that the elastic accommodation stress field surrounding the transformed plates is responsible for the athermal component of interface friction. (The range of the accommodation stress field is comparable to the diameter of an isolated plate of shear, taken as the grain size d.)

(2) Shape Accommodation

Our observations of shape memory effects in Ce-TZP imply that the primary modes of shape accommodation in t-to-m transformation are twinning and elastic distortion. Thus, transformation plasticity in Ce-TZP is indeed due to the t-to-m transformation, with an insignificant contribution from dislocation slip. In a parallel study of Mg-PSZ, we found that approximately 70% of the shape strain was recoverable during heating and that the texture was reversible. (In Mg-PSZ, no burst in forward or reverse transformation was resolvable. We recall that in Ce-TZP, shape memory persisted even after heavy deformation, when the microstructure resembles a dispersed tetragonal phase PSZ more than a homogeneous phase TZP. Hence, the shape memory effects and the dominance of elastic accommodation in t-to-m transformation at lower temperatures are probably general features for zirconia polycrystals, over a wide range of grain sizes, phase distributions, and stress states.

Cycling experiments revealed another mode of accommodation, namely, the microcracking which led to specimen failure after a few cycles. This is hardly surprising. Our experience with zirconia found that microcracking is an unavoidable consequence of transformation. For example, we reported elsewhere the reduction of elastic constants following deformation which occurs from grain-boundary cracking.[1] Yu, Chiao, and Chen also reported microcracking in skull melt ZrO_2 due to an orthorhombic-to-monoclinic transformation, and in transformed overaged Y-TZP.[29] In a thermal cycling experiment which we will not detail here, we found the specimen fractured into several pieces after five cycles between M_b and A_b. Amazingly, despite microcracking, shape memory effects were not affected in a significant way by the occurrence of microcracking. We can only conclude that, although detrimental to stiffness, strength, and structural integrity, microcracking in Ce-TZP is not important for shape accommodation.

The dominance of elastic accommodation simply reflects the difficulty of dislocation activity in zirconia, at least at the level of macroscopic flow stresses encountered in Ce-TZP and Mg-PSZ at lower temperatures under various stress states, i.e., up to 2.5 GPa. Recently, Lankford *et al.* found that dislocation plasticity is present but limited in Y-PSZ single crystals at room temperature, but not in fine-grain Y-TZP.[30] The room-temperature critical resolved shear stress for slip in these experiments was at least 1 GPa if not much higher.[30] There seems to be little doubt that the intrinsic difficulty of the operation of dislocations, compounded by the strengthening effect of a fine-grain polycrystal, should effectively prevent the occurrence of dislocation plasticity in most transformation-toughened zirconia systems. The above observation stands despite the definitive experimental evidence that dislocations *extrinsically introduced via radiation damage* act as potent nucleation sites in pure, highly metastable ZrO_2 small single crystals.[13] Inasmuch as extrinsically introduced dislocations are not necessarily mobile and most likely unavailable in normal circumstances, plasticity in these materials at lower temperature is only via transformation plasticity, which involves martensitic transformation, twinning, and elastic distortion, but not dislocation slip.

At this point, it is instructive to reflect on the large body of literature on shape memory alloys and ferrous martensites,[2,3] to compare and contrast the present shape memory effects found in a ceramic. For metals and alloys, it has been concluded that the burstlike transformation and the shape memory effects are mutually exclusive.[2] The reason is probably due to the large plastic deformation via dislocation slip which accompanies burstlike transformation, thus rendering the reverse motion of the interface extremely difficult. Such mutual exclusion does not hold in ceramics, for significant dislocation activity is substantially absent at low temperatures. To facilitate elastic accommodation without plastic deformation, maintaining a low elastic constant but raising the flow stress has been found very effective.[16,17] Ordered alloys, which possess these attributes, indeed constitute the majority of shape memory alloys known to date.[2,3] In this regard, ceramic martensites as a class would have been natural candidates for shape memory alloys — if only grain and interface cracking could be mitigated.

The above picture is based on a nucleation-controlled autocatalysis model[1] for cooling toward M_b and a growth-controlled single-plate model[16,17] for cooling below M_b and for subsequent heating (see Figs. 1 and 15). Although the single-plate model is an oversimplification, it captures the essence of thermoelastic equilibrium in martensitic transformation and correctly predicts both the burst behavior in the reverse martensitic transformation at A_b and its grain size dependence. Attempts to introduce other considerations to modify the single-plate geometry are numerous in the shape memory alloy literature. For zirconia, Coyle[4] and Evans and Cannon[5] have also qualitatively depicted the myriad of possible internal structures of multiple variants and their associated

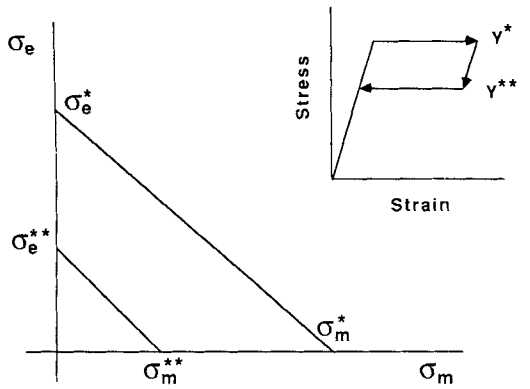

Fig. 16. Schematic pseudoelastic stress–strain curve and yield loci.

stress–strain behaviors. While it is not the intent of the present study to provide the necessary information to critically test the above conjectures, it is justified to acknowlege that multiple variants tend to partially accommodate their mutual shape strains by assuming appropriate orientations, resulting in an internal stress field of a lower magnitude and a shorter range. The consequent lowering of the strain energy of the system should stabilize the monoclinic phase to a higher A_b, although the partial recovery below A_b due to plate thinning could also be facilitated by less friction. To the extent that microcracking is occasionally and locally important as an accommodation mechanism, it should have a similar effect on alleviating internal stresses. These complicated aspects will figure most prominently in the heavily or cyclically deformed ceramics.

(3) Implications on Transformation Plasticity and Transformation Toughening

Stress-assisted transformation plasticity generally follows a shear-dilatant yield criterion.[1,9] In the previous paper, we have determined the critical effective stress σ_e^* and the critical mean stress σ_m^*, from yielding experiments conducted under various stress states.[1] Although the shape memory effects have been investigated mostly in the compression regime, the characteristics of stress-assisted transformation seem to be preserved, as evidenced by the positive temperature dependence of the yield stress and the partitioning of the deviatoric and volumetric strains. Referring to an idealized pseudoelastic stress–strain curve shown in Fig. 16, we may thus assign a second set of critical stresses, denoted by σ_e^{**} and σ_m^{**}, to the condition when plastic strains revert. A modified yield locus to incorporate both transformation plasticity and pseudoelasticity is also illustrated in Fig. 16. Within the spirit of stress-assisted transformation,[1] the same mechanical driving force is expected to be responsible for both forward and reverse transformations. The roughly similar strain partitioning in transformation plasticity at low temperature and in forward and reverse pseudoelasticity at high temperature seems to further suggest, by virtue of the "normality rule" in plasticity,[1] that the ratios of σ_e^*/σ_m^* and $\sigma_e^{**}/\sigma_m^{**}$ are nearly equal. The ratio of σ_e^{**}/σ_e^* or, equivalently, σ_m^{**}/σ_m^*, of course, is an increasing function of temperature, bounded between zero and unity.

It is apparent from the inset in Fig. 16 that the work of plastic dissipation is the area circled by the hysteresis loop in pseudoelasticity. Thus, pseudoelastically deformed and unloaded materials still dissipate energy, but no net shape change or phase change can be detected in the end. The existence of plastic dissipation implies that "pseudoelastic toughening" can occur, even though no permanent transformation zone remains near the fracture surface. It was this realization which led Coyle[4] to suspect that transformation toughening occurred in his Ce-TZP materials. Based on Coyle's observation, a model of dilatation toughening for reversible *t*-to-*m* transformation was proposed previously.[5] This model is modified below to account for the toughening contribution from shear.

Following the derivation of the modified McMeeking–Evans equation[31] using the shear-dilatant yield criterion,[18,32] we can easily show that the toughness increment by "pseudoelastic toughening" is

$$\Delta K = 0.48 E f k e_T^* h^{1/2}/(1 - \nu) \tag{7}$$

where k is given by $1 - \sigma_e^{**}/\sigma_e^*$, and the other quantities have been previously defined in the companion paper.[1] When transformation becomes irreversible at lower temperatures, k equals unity and the above equation reduces to Eq. (18) in the previous paper for transformation plasticity. Although the transformation zone in Eq. (7) refers to the condition when the σ_e^*–σ_m^* yield locus is exceeded at the crack tip under load, it disappears once the load is released upon fracture. For this reason and the lack of information on k in most cases, the application of Eq. (7) to simple fractography measurements will involve substantial experimental difficulty.

VI. Summary

Experimental results and theoretical analysis presented in this and the previous paper[1] have identified the following as the central aspects of transformation plasticity in Ce-TZP, as it relates to transformation and transformation toughening.

Phase connectivity is determined by the tetragonal phase only. Characteristics of transformation and deformation in a homogeneous TZP are fundamentally altered when the phase connectivity is interrupted by a second non-zirconia phase or a nontransformable phase.

Stress assistance is provided by the coupling of the applied stresses and the transformation strains. Both a deviatoric and a volumetric component are involved. The stress assistance determines the stress-state sensitivity, the temperature sensitivity, and brings about pseudoelastic transformation plasticity above A_b.

Strain accommodation is primarily by variant arrangement and elastic distortion; both are reversible despite some frictional resistance. When a stress assistance is provided, the strain accommodation is further reflected in the orientation distribution of both *t* and *m* variants, producing a distinct texture and a strain partition consistent with the shear-dilatant yield criterion.

Thermoelastic equilibrium is a consequence of the dominance of elastic accommodation. It determines the stability of the existing monoclinic variants and possibly influences the elastic interactions among variants. The grain size dependence of A_b can be explained by this concept.

Nucleation statistics of both single- and multiple-site nucleation are dependent on the driving force and dictate a size effect. They also determine the stability of the metastable tetragonal phase. The grain size dependence of M_b and the microstructure dependence of autocatalysis are dictated by this statistical consideration.

Autocatalysis occurs during cooling and in deformation. To effect multiple-site nucleation, a large chemical driving force is more essential than a large mechanical driving force, because the stress assistance is not the same among variants of different orientations. When the chemical driving force is low, no autocatalysis should occur in TZP despite a much higher flow stress.

Flow localization during deformation in the autocatalytic regime proceeds via dilatant shear bands. Fracture originates from these bands. At higher temperatures and in dispersed tetragonal polycrystals, no flow localization is macroscopically evident.

Microcracking occurs at grain boundaries during transformation. Although demonstrably unimportant for shape accommodation, the accumulated damage weakens the structure and leads to rapid failure.

Toughenability can be enhanced by both transformation plasticity at lower temperature and pseudoelasticity at higher temperatures. In most cases, however, the McMeeking–Evans equation cannot be used to relate the process zone size.

APPENDIX

The evaluation of strain energy of an inclusion follows the standard Eshelby procedure, which is outlined elsewhere.[23] For the present case, it has been shown,[5] by simplifying the solution in Ref. 16, that g_{str} and K are given by

$$g_{str} = [1/(1 - \nu)]\mu(e_{yy}^2 + 2\nu e_{yy}e_{zz} + e_{zz}^2) \quad \text{(A-1)}$$

$$K = \pi\mu[16(2 - \nu)e_{xz}^2 + 8e_{xx}^2 - 13(e_{yy}^2 + e_{zz}^2) - 2(16\nu - 1)e_{yy}e_{zz} + 8(1 + 2\nu)(e_{yy} + e_{zz})e_{xx}]/32(1 - \nu) \quad \text{(A-2)}$$

In the above, μ is the shear modulus, ν is the Poisson ratio, the major t-to-m shear is e_{xz}, and the remaining distortions are dilatations along **x**, **y**, and **z** given by e_{xx}, e_{yy}, e_{zz}.

Among the above strains, e_{xz} and e_{xx} can be accommodated as an invariant plane strain (IPS) on the habit plane.[23] Thus, the monoclinic plate chosen here satisfies a near-IPS configuration. Moreover, coherency across the habit plane can be maintained if the plane coincides with a cystallographic plane. Then it also has a low interfacial energy. The non-IPS strain energy g_{str} derived from e_{yy} and e_{zz} is relatively small and enters, along with g_{ch}, as a volume-proportional free energy contribution into Eq. (1).

Acknowledgment: We are grateful for useful discussions with Dr. K. J. Bowman.

References

[1]P. E. Reyes-Morel and I-W. Chen, "Transformation Plasticity of Ce-TZP: I, Stress Assistance and Autocatalysis," *J. Am. Ceram. Soc.*, **71** [5] 343–53 (1988).
[2]L. Delaey, R. V. Krishnan, H. Tas, and H. Walimont, "Review—Thermoelasticity, Pseudoelasticity and the Memory Effects Associated with Martensitic Transformations," *J. Mater. Sci.*, **9** [9] 1521–55 (1974).
[3]K. Otsuka and K. Shimizu, "Pseudoelasticity and Shape Memory Effects in Alloys," *Int. Met. Rev.*, **31** [3] 93–114 (1986).
[4]T. W. Coyle, "Transformation Toughening and Martensitic Transformation in ZrO_2"; Sc.D. Thesis. Department of Materials Science and Engineering, Massachusetts Institute of Technology, Cambridge, MA, Feb. 1985.
[5]A. G. Evans and R. M. Cannon, "Toughening of Brittle Solids by Martensitic Transformations," *Acta Metall.*, **34** [5] 761–800 (1986).
[6]D. B. Marshall and M. R. James, "Reversible Stress-Induced Martensitic Transformation in ZrO_2," *J. Am. Ceram. Soc.*, **69** [3] 215–17 (1986).
[7]D. B. Marshall, "Strength Characteristics of Transformation-Toughened Zirconia," *J. Am. Ceram. Soc.*, **69** [3] 173–80 (1986).
[8]M. V. Swain, "Shape Memory Behavior in Partially Stabilized Zirconia Ceramics," *Nature (London)*, **322**, 234 (1986).
[9]I-W. Chen and P. E. Reyes-Morel, "Implications of Transformation Plasticity in ZrO_2-Containing Ceramics: I, Shear and Dilatation Effects," *J. Am. Ceram. Soc.*, **69** [3] 181–89 (1986).
[10]R. H. J. Hannink, J. R. Porter, and D. B. Marshall, "Direct Observation of Cyclic Phase Transformations in Zirconia," *J. Am. Ceram. Soc.*, **69** [6] C-116–C-119 (1986).
[11]I-W. Chen and Y-H. Chiao, "Martensitic Nucleation in ZrO_2," *Acta Metall.*, **31** [10] 1627–38 (1983).
[12]I-W. Chen and Y-H. Chiao, "Martensitic Transformation in ZrO_2 and HfO_2—An Assessment of Small Particle Experiments with Metal and Ceramic Matrices"; pp. 33–45 in Advances in Ceramics, Vol. 12, Science and Technology of Zirconia II. Edited by N. Claussen, M. Rühle, and A. H. Heuer. American Ceramic Society, Columbus, OH, 1984.
[13]I-W. Chen and Y-H. Chiao, "Theory and Experiment of Martensitic Nucleation in ZrO_2-Containing Ceramics and Ferrous Alloys," *Acta Metall.*, **33** [10] 1827–45 (1985).
[14]Y-H. Chiao, "Nucleation and Growth Processes of Martensitic Transformation in ZrO_2 Particles"; Ph.D. Thesis. Department of Materials Science and Engineering, Massachusetts Institute of Technology, Cambridge, MA, Sept. 1986.
[15]I-W. Chen, Y-H. Chiao, and K. Tsuzaki, "Statistics of Martensitic Nucleation," *Acta Metall.*, **33** [10] 1847–59 (1985).
[16]G. B. Olson and M. Cohen, "Thermoelastic Behavior in Martensitic Transformation," *Scr. Metall.*, **9** [11] 1247–54 (1975).
[17]G. B. Olson and M. Cohen, "Reply to 'On the Equilibrium Temperature in Thermoelastic Martensitic Transformations,'" *Scr. Metall.*, **11** [5] 345–47 (1977).
[18]P. E. Reyes-Morel, "An Experimental Study of Constitutive Relations of Transformation Plasticity in Zirconia-Based Ceramics"; Ph.D. Thesis. Department of Nuclear Engineering, Massachusetts Institute of Technology, Cambridge, MA, June 1986.
[19]M. S. Paterson, Experimental Rock Deformation—The Brittle Field. Springer-Verlag, West Berlin, Federal Republic of Germany, 1978.
[20]B.-S. Li, J.-S. Cherng, K. J. Bowman, and I-W. Chen, "Domain Switching as a Toughening Mechanism in Tetragonal Zirconia," *J. Am. Ceram. Soc.*, **71** [7] C-362–C-364 (1988).
[21]K. J. Bowman and I-W. Chen, "Deformation Texture of Transformation Toughened Zirconia"; in Proceedings of International Conference on Textures of Materials, TMS-AIME. Edited by U. F. Kocks and J. Kallend. The Metallurgical Society of AIME, New York, 1987.
[22]P. E. Reyes-Morel, "Low Temperature Creep and Isothermal Transformation of Mg-PSZ," paper No. 177-B-87, 87th Annual Meeting of the American Ceramic Society, Pittsburgh, PA, April 26–30, 1987.
[23]J. W. Christian, The Theory of Transformations in Metals and Alloys, 2nd ed.; Vol. 1. Pergamon, New York, 1975.
[24]L. Kaufman and M. Cohen, "Thermodynamics and Kinetics of Martensite Transformations," *Prog. Met. Phys.*, **7**, 165–246 (1958).
[25]V. Raghavan and M. Cohen, "A Nucleation Model for Martensitic Transformations in Iron-Base Alloys," *Acta Metall.*, **20** [3] 333–38 (1972).
[26]E. Tani, M. Yoshimura, and S. Somiya, "Revised Phase Diagram of the System ZrO_2–CeO_2 below 1400°C," *J. Am. Ceram. Soc.*, **66** [7] 506–10 (1983).
[27]Y-H. Chiao and I-W. Chen, "In-Situ Observations of the Structures and Migration of Martensitic Interface in Small ZrO_2 Particles," *Trans. Jpn. Inst. Met. Suppl.*, **27**, 197–203 (1986).
[28]U. F. Kocks, A. S. Argon, and M. F. Ashby, "Thermodynamics and Kinetics of Slip," *Prog. Mater. Sci.*, **19**, 1 (1975).
[29]I-W. Chen; unpublished work.
[30]J. Lankford, L. Rabenberg, and R. Page, "Deformation Mechanisms in Yttria-Stabilized Zirconia"; unpublished work.
[31]R. McMeeking and A. G. Evans, "Mechanisms of Transformation Toughening in Brittle Materials," *J. Am. Ceram. Soc.*, **65** [5] 242–45 (1982).
[32]I-W. Chen and P. E. Reyes-Morel, "Transformation Plasticity and Transformation Toughening in Mg-PSZ and Ce-TZP"; pp. 75–88 in Advanced Structural Ceramics, Materials Research Society Symposium Proceedings Series, Vol. 78. Edited by P. F. Becher, M. V. Swain, and S. Somiya, Materials Research Society, Pittsburgh, PA, 1986. □